Geochemistry, Geophysics, Geosystems

RESEARCH ARTICLE
10.1029/2020GC009504

Key Points:

- Results of micromagnetic multilayer core-shell models agree well with experimental observations of low temperature oxidized magnetite
- The variation of hysteresis parameters with the oxidation state is consistent with the existence of a magnetic unstable zone
- The effective identification of the magnetic unstable zone should improve the consistent observation of paleomagnetic signals from geological samples

Supporting Information:

- Supporting Information S1

Correspondence to:
K. Ge,
kunpeng.ge@yahoo.com

Citation:
Ge, K., Williams, W., Nagy, L., & Tauxe, L. (2021). Models of maghematization: Observational evidence in support of a magnetic unstable zone. *Geochemistry, Geophysics, Geosystems*, *22*, e2020GC009504https://doi.org/10.1029/2020GC009504

Received 30 OCT 2020
Accepted 23 JAN 2021

Models of Maghematization: Observational Evidence in Support of a Magnetic Unstable Zone

Kunpeng Ge[1], Wyn Williams[2], Lesleis Nagy[3], and Lisa Tauxe[3]

[1]School of Geophysics and Measurement-control Technology, East China University of Technology, Nanchang, China, [2]School of GeoSciences, University of Edinburgh, Edinburgh, UK, [3]Geosciences Research Division, Scripps Institution of Oceanography, La Jolla, CA, USA

Abstract Recent micromagnetic simulations predict that particles have an abnormal region of low magnetic stability for grain sizes near the domain state transitions from single domain to single vortex. The implications of this zone are not yet fully understood, but if the size range of this window changes as a function of applied field and temperature then it is likely to contribute to observational uncertainties in paleomagnetic recordings. The narrow size range of this zone means that its effects are difficult to identify when integrated across the much wider distribution of grain sizes present in a sample. Here we report a method of examining the unstable region using low temperature oxidation of magnetite. The rock magnetic experiments on partially oxidized particles with a median diameter close to the unstable zone are reinterpreted using micromagnetic simulations of a multilayer core-shell structure. The predicted magnetic properties exhibit significantly improved agreement with experimental data than that of the previously reported single core-shell coupled geometry. The observed changes in remanence and coercivity are associated with predicted domain structure changes near a proposed magnetic unstable zone (~80–~120 nm), and so provide the first experimental indication of the existence of such a region. We also demonstrate that magnetic remanence in particles with grain sizes outside this size range were stable to maghemitization. The research provides ideas for the experimental study of the "magnetic unstable zone" and is significant to the correct interpretation of magnetic recordings. Finally, the partially oxidized magnetite particles are able to record paleomagnetic signals.

Plain Language Summary Magnetic minerals in geological samples can record variations of the geomagnetic field over billions of years and provide a way to investigate the evolution of the Earth. The recording ability of minerals varies with grain size and decreases for both the largest and smallest grains. Recent numerical models suggest that even within the intermediate grain sizes previously regarded as good recorders, there exists an unstable region whose characteristics are not yet fully understood. This prediction is of paramount importance for the fundamental accuracy of paleomagnetic studies, because by identifying and excluding such unstable recorders it is possible to increase the accuracy of paleointensity determinations. This study provides the first experimental evidence in support of the existence of the unstable zone.

1. Introduction

Paleomagnetic studies contribute fundamentally to our understanding of plate tectonics, reconstruction of a global climate framework, the physics of dynamic processes deep within the Earth as well as providing constraints on theories of evolution of galaxies (Bloxham, 2000; Gubbins et al., 2011; Labrosse et al., 2001; Tarduno et al., 2015; H. Wang et al., 2017). The goal of paleomagnetism is to extract recorded magnetic information from geological samples. However, these recordings are controlled by many factors, such as the type of magnetic minerals, grain size and morphology, intergrain magnetic interactions and chemical alteration (Dunlop & Özdemir, 1997). In order to improve the accuracy of interpretations of magnetic recordings and geological implications, systematic experiments and numerical simulations are necessary to decouple the effects of physical parameters on paleomagnetic signals (Ge & Liu, 2014; Muxworthy et al., 2003; Schabes & Bertram, 1988; Williams & Dunlop, 1989).

The traditional understanding of rock magnetism has evolved with the development of publicly available code for numerical micromagnetic modeling (Conbhuí et al., 2018). For instance, Schabes and Bertram (1988)

and Williams and Dunlop (1989) found that the structure traditionally called pseudo-single-domain (PSD) that exists in grain sizes slightly larger than uniformly magnetized single domain (SD) grains, is commonly either a flower state (*F*) or a single vortex (SV) state, with grain sizes ranging from ~80 nm up to 1,000 nm, after which the multivortex (MV) and multidomain (MD) structures eventually form. These model predictions, combined with the evidence of SV from electron-holographic imaging (Almeida et al., 2016), have re-defined our understanding of domain state evolution and magnetic recording fidelity.

Nagy et al. (2017) recently reported a grain size range with unexpectedly low magnetic stability that exists at the SD/SV boundary, equivalent to grain sizes of ~84 nm–100 nm for equal-dimensional grains of magnetite. This low stability zone is characterized by a multiplicity of possible domain states such as a hard axis aligned SV (HSV), easy axis aligned SV (ESV), or easy axis aligned SD structure. Significantly, the energy barriers between these domain states are small enough that they are unstable or only weakly stable at room temperature. Moreover, the location and width of the unstable zone depends upon mineralogy and grain morphology (Nagy et al., 2019). Although the implications of these unstable zones for paleomagnetic observations are not yet fully understood, it is possible that they play an important role in degrading paleomagnetic recordings through undesirable effects such as pTRM tails where the blocking and unblocking temperatures are different (Shashkanov & Metallova, 1972; Santos & Tauxe, 2019; Shaar & Tauxe; 2015; Yu et al., 2013). Direct observation of such an unstable region, however, is hampered by its narrow grain-size range and its effects are difficult to isolate from the total sample magnetic remanence. One possible solution is to use low-temperature oxidation on laboratory grown samples with a mean grain size near the unstable zone for magnetite. As oxidation proceeds there should be a shift in the proportion of SD, HSV and ESV domain states contributing to the observed remanence which we can predict and compare with the experimental observations.

Low temperature oxidation is of great interest to paleomagnetic studies because of its widespread occurrence in nature (Moskowitz, 1980; Özdemir & Dunlop, 2010; van Velzen & Dekkers, 1999). It has been shown that the oxidation process of magnetite grains to maghemite is controlled by diffusion of iron cations (O'Reilly, 1984), and further driven by the variation of Fe^{2+} density from interior to the rim that eventually produces an oxidation gradient within the grain (Özdemir & Dunlop, 2010). Based on the diffusion process of iron cations, the oxidation of single magnetite crystals occurs continuously and nonlinearly from the surface of the grain to the interior (Gallagher et al., 1968; O'Reilly, 1984; see in Methods). Although oxidation produces little change of the particle size, oxidation does reduce the magnetization, which changes domain state energies and thus the location of the low stability zone and critical grain sizes that mark the boundary between the SD, HSV and ESV domain states. Therefore, for a distribution of magnetite particles with a median particle size near the predicted room temperature unstable zone, the gradual change of magnetic characteristics during low temperature oxidation will sweep the peak of unstable zones through the distribution of particles in the sample.

In this study, we investigate the change in domain structures and magnetic properties as a function of oxidation state. We focus on the paleomagnetically significant SD and SV grain size range boundary, and where the oxidation is assumed to occur across a finite width of grain. With a multilayer finite element approach using the modeling package MERRILL (Micromagnetic Earth Related Rapid Interpreted Language Laboratory; Conbhuí et al., 2018), the inclusion of an oxidation gradient in the model provides a realistic comparison to the experimental data. Combined with multilayer models, the experimental observations are consistent with the rapid change in magnetic domain state that is associated with the magnetic unstable zone. The significance of identifying the unstable zone by low temperature oxidation for magnetic recordings of geological samples is also discussed.

2. Methods

2.1. Construction of the Model

The experimental data of synthetic reduced and oxidized magnetite have been previously described by Ge et al. (2014). Transmission electron microscopy (TEM) and grain size distributions for the reduced magnetite grains are shown in Figure 1. The statistical median grain size and the axial ratio (major axis/minor

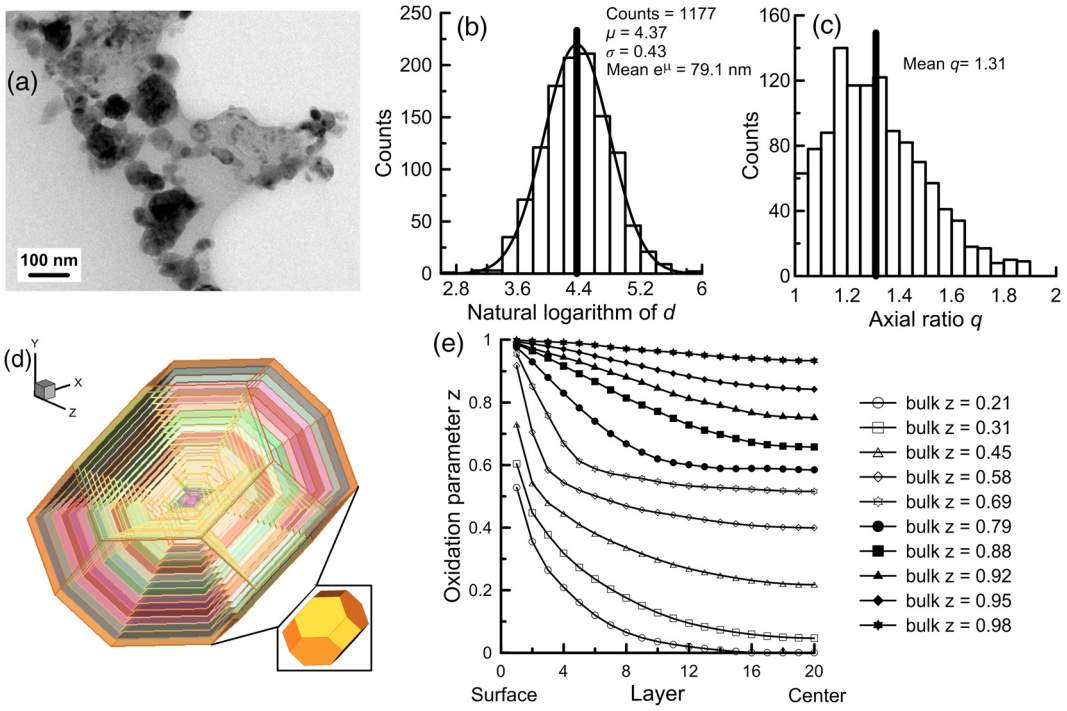

Figure 1. Frames of reference for micromagnetic modeling. TEM image (a) and observed grain size distributions of magnetite powder 4,000 (b)–(c) (modified from Ge et al., 2014). The black curve in (b) represents a normal distribution fit of the histograms to the logarithm of the grain size. μ andσ are the average value of logarithm of grain size and the standard deviation respectively. The mean axial ratio q is of 1.31, and is shown in distribution of axial ratio (c) with thick black lines. (d) The interior 20 layers modeling a multilayer core-shell as a gradual transition zone using a translucent view, for the truncated octahedron core-shell model with an elongation direction and factor of (111) and 1.31 respectively. (e) Oxidation parameter z as a function of layer for different oxidation stage of bulk magnetite grain (modified from Gallagher et al. (1968)).

axis) are 79.1 nm and 1.31, respectively. The low temperature oxidized magnetite was obtained by heating reduced magnetite to different temperatures for various periods of time, and the degree of oxidation was determined by a fitting of the standard curves of cell size obtained from XRD observation versus oxidation parameter z (Readman & O'Reilly, 1972).

The numerical micromagnetic models used a truncated octahedron particle shape, with an elongation parameter of 1.31 along the (111) direction typical of that seen in the experimental data (Figure 1). To approach a continuously oxidized core-shell structure illustrated by Gallagher et al. (1968) by discretization methods, an oxidation transition zone was generated by up to 20 concentric zones of similar geometry to the grain, but of decreasing volume so that the thickness of each zone was identical.

In the micromagnetic modeling, the material parameters appropriate to magnetite at room temperature were used, namely exchange constant ($A_{ex} = 1.33 \times 10^{-11}$ Jm^{-1}), magnetocrystalline anisotropy ($K_1 = -1.24 \times 10^4$ Jm^{-1}) and saturation magnetization ($M_s = 4.8 \times 10^5$ Am^{-1}) (Pauthenet & Bochirol, 1951; Heider & Williams, 1988). For maghemite, the corresponding principle magnetic parameters applied in this core-shell model are $1 \times 10^{-11} Jm^{-1}$, -4.6×10^3 Jm^{-1}, and 3.8×10^5 Am^{-1} respectively (Dunlop & Özdemir, 1997). It is important to note that magnetite and maghemite share the same cubic crystalline axis.

Using Fick's law of diffusion, Gallagher et al. (1968) calculated the continuous concentration profiles of Fe^{2+} cation (oxidation state) from outer to inner of a magnetite particle corresponding to successive bulk oxidation stages (Figure 1). The material parameters for each of the partially oxidized layers of the core-shell model were determined by a simple linear interpolation of the material parameters of magnetite and maghemite on the basis of their oxidation state. An exchange parameter is required at the boundary between the

layers of different oxidations sate, and this was simply the average of the exchange constant of neighboring layers (Ge et al., 2014).

The bulk oxidation parameters were determined by simply performing the volume average of the oxidation state of each zone. In this study, grains of 10 different average oxidized states were modeled with bulk z-values of 0.21, 0.31, 0.45, 0.58, 0.69, 0.79, 0.88, 0.92, 0.95, and 0.98, extracted from the numerical kinetic model of Gallagher et al. (1968), and then inputinto the micromagnetic calculation. Including the two end members ($z = 0$ for magnetite, and $z = 1$ for maghemite), a total of 12 different oxidation states were calculated. Nine different grain sizes were considered, each of truncated octahedron in shape, with volumes equivalent to cubes with edge lengths of 40, 60, 70, 80, 90, 100, 120, 140, and 160 nm respectively. In all, 108 core-shell models with varied oxidation states and grain sizes were obtained.

2.2. Micromagnetic Modeling

The calculation of the core-shell structure was performed using MERRILLv1.4 (Micromagnetic Earth Related Rapid Interpreted Language Laboratory) (Conbhuí et al., 2018), which is capable of modeling multiphase magnetic materials in grains of arbitrary shape. Simulations of hysteresis were conducted with applied field varying from 180 mT to −180 mT in steps of 5 mT, with applied fields aligned along (111), (100), and (110) directions. The initial magnetization state for each half-loop of the hysteresis was set to be saturated (uniformly magnetized state) in the direction of the applied field. Reported values for the coercivity (B_c) and ratio of saturation remanence to saturation magnetization (M_{rs}/M_s) are the average of those along the three applied field directions.

3. Results

3.1. Hysteresis Parameters

The typical hysteresis curves of grains of different size versus oxidation are shown in Figure 2. On the whole, the hysteresis loops of particles show a systematic change with the increase of oxidation state (Supporting Information Figure S1). The 60 nm grains exhibit typical SD characteristics, with stable M_{rs}/M_s and slight decreasing B_c during oxidation. The predicted M_{rs}/M_s value of ∼0.8 for these SD grains reflects the contribution from both shape and crystalline anisotropy, whose dominance would produce a value of 0.5 and 0.866 respectively.

For lager grains, the 90 nm grains exhibit both an evident variation of B_c and M_{rs}/M_s as the oxidation proceeds, while the SD behaviors are preserved to some extent (Supporting Information Figure S2). Figure 3 shows the detailed variations of B_c and M_{rs}/M_s as a function of oxidation parameter. For 100 nm sized grain, the SD behavior disappears, and the hysteresis parameters also varied dramatically. Much larger grains (140 nm) begin to preserve stable B_c and M_{rs}/M_s regardless of the chemical alteration.

For grains in the SD range from 40 nm to 70 nm, B_c decreases gradually and M_{rs}/M_s remains constant as oxidation increases. The hysteresis behavior of slightly larger grains, in the SV domain state (80–120 nm) begins to show a greater variability as a function of oxidation. It appears that B_c for ≥80 nm grains and M_{rs}/M_s for ≥90 nm grains oscillate during oxidation, with dramatic increases and decreases seen at the early and late stage of oxidation, respectively. This is a reflection of the fact that grains lie near the unstable zone boundary, where the multiplicity of domain states and rapidly changing thermal stability and coercivity will make their magnetic characteristics sensitive to changes in oxidation. In contrast, for larger SV grains (140–160 nm) the parameters remain nearly unchanged. Specifically, B_c decreases slightly, while M_{rs}/M_s shows a slight increase as the oxidation proceeds.

3.2. Micromagnetic Structures

The micromagnetic structures of the multilayer core-shell model are displayed in Figures 4 and 5. Figure 4 shows zero-field micromagnetic core-shell structures for 60 nm grains with the degree of oxidation (z) equal

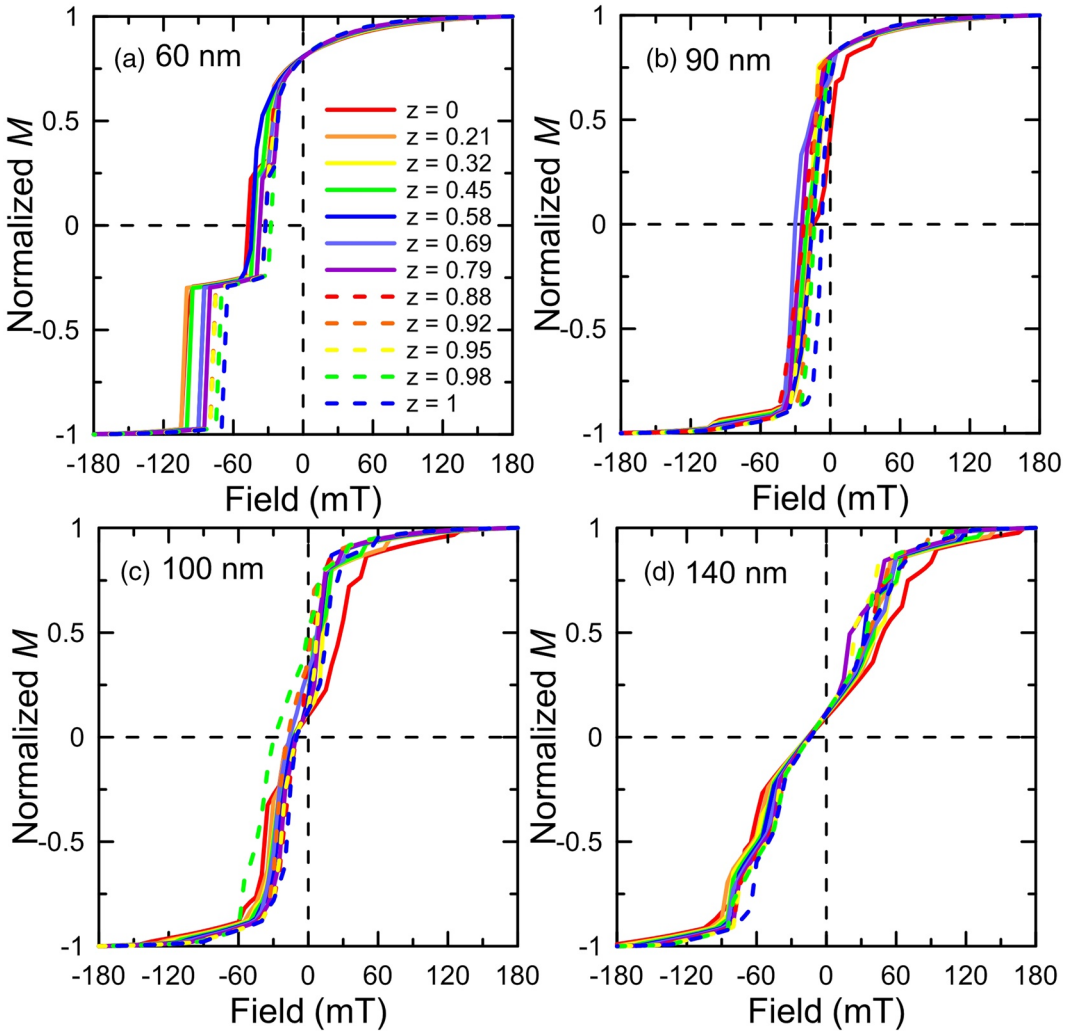

Figure 2. Hysteresis curves (formed from the average of curves for fields applied the (100), (110), and (111) directions) for 60, 90, 100, and 140 nm sized grains, as a function of grain oxidation parameter, z. The magnetizations are normalized to that of a uniformly magnetized particle.

to 0, 0.45, and 1, respectively. As can be seen from the direction of magnetization vectors, the remanence remains in a nearly uniform SD state during the entire oxidation process. Similarly, for grains larger than 140 nm, the (111) aligned vortex structure (isosurfaces in Figures 4d–4f) remains almost unchanged both in value and direction of helicity throughout the low-temperature oxidation.

In contrast, the smaller SV grain sizes (90–100 nm) exhibit a more complex behavior, where the volume ratio of vortex core to total volume for particles increases (Figure 5), while the magnetic behavior during oxidation is more complicated. For instance, the stoichiometric 90 nm sized magnetite shows a $\left(11\,\bar{1}\right)$ (hard) aligned vortex core, typical of unstable domain states found near the SD/SV grain size boundary (Nagy et al., 2017, 2019). As the oxidation parameter increases, the magnetization structure moves away from this boundary and switches to a nearly uniform domain state at an early oxidation stage of $z = 0.21$, and remains in this state during further oxidation. Similarly, the 100 nm grain has a hard aligned $\left(11\,\bar{1}\right)$ SV state for stoichiometric magnetite which remains up to $z = 0.45$ at which point the vortex core becomes curved and switches to an intermediate (110) direction as the oxidation parameter z approaches 0.79, and subsequently to an easy axis (111) at $z = 0.98$ before finally returning to the initial $\left(11\,\bar{1}\right)$ direction when the particle is totally oxidized to maghemite.

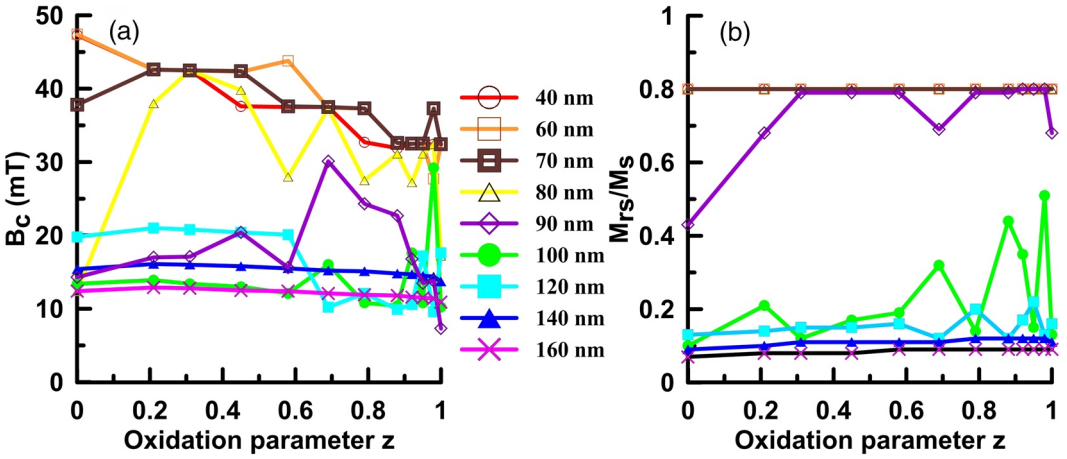

Figure 3. Micromagnetic results of (a) coercive field (B_c) and (b) ratio of saturation remanence to saturation magnetization (M_{rs}/M_s) versus oxidation parameter z for multilayer core-shell models. Note that curves of 40, 60, 70, 80 nm grains in (b) are completely overlapped with a constant (M_{rs}/M_s) value of ~0.8 throughout the oxidation process.

4. Discussion

Magnetite powder is difficult to disperse because of its high interparticle magnetostatic interaction strength between grains and these interactions will impact the observed values of the hysteresis behavior. Muxworthy et al. (2003) modeled these interactions in clusters of grains, and demonstrated that even after 1%

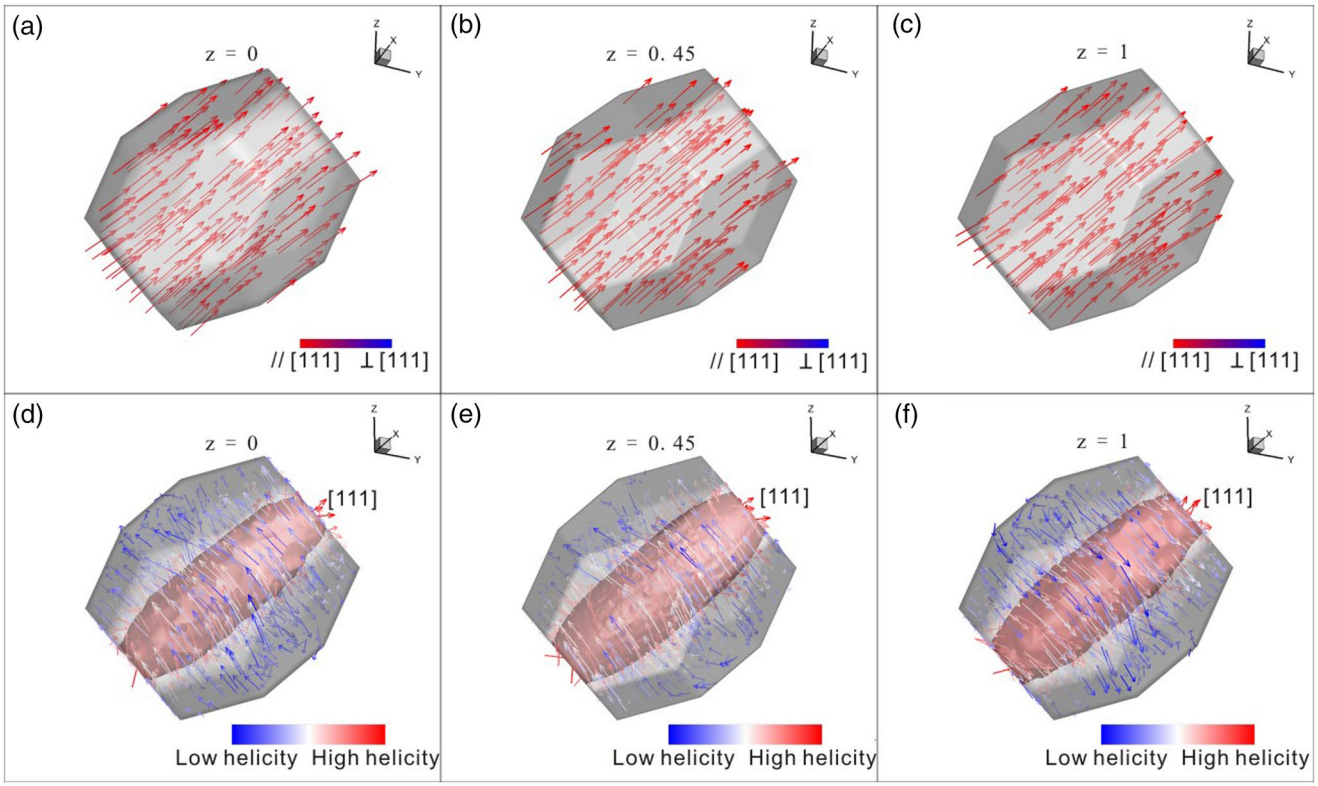

Figure 4. Micromagnetic structures for grain size of 60 nm (a–c) and 140 nm (d–f) particles at zero field, as a function of oxidation parameters, equal to $z = 0$, $z = 0.45$, and $z = 1$. The initial applied field for all models shown here was saturated along the (111) direction. (a–c) Show the magnetization vectors colored red parallel to (111) and blue perpendicular to (111). (d–f) display the helicity isosurfaces that correspond to the regions surrounding vortex cores.

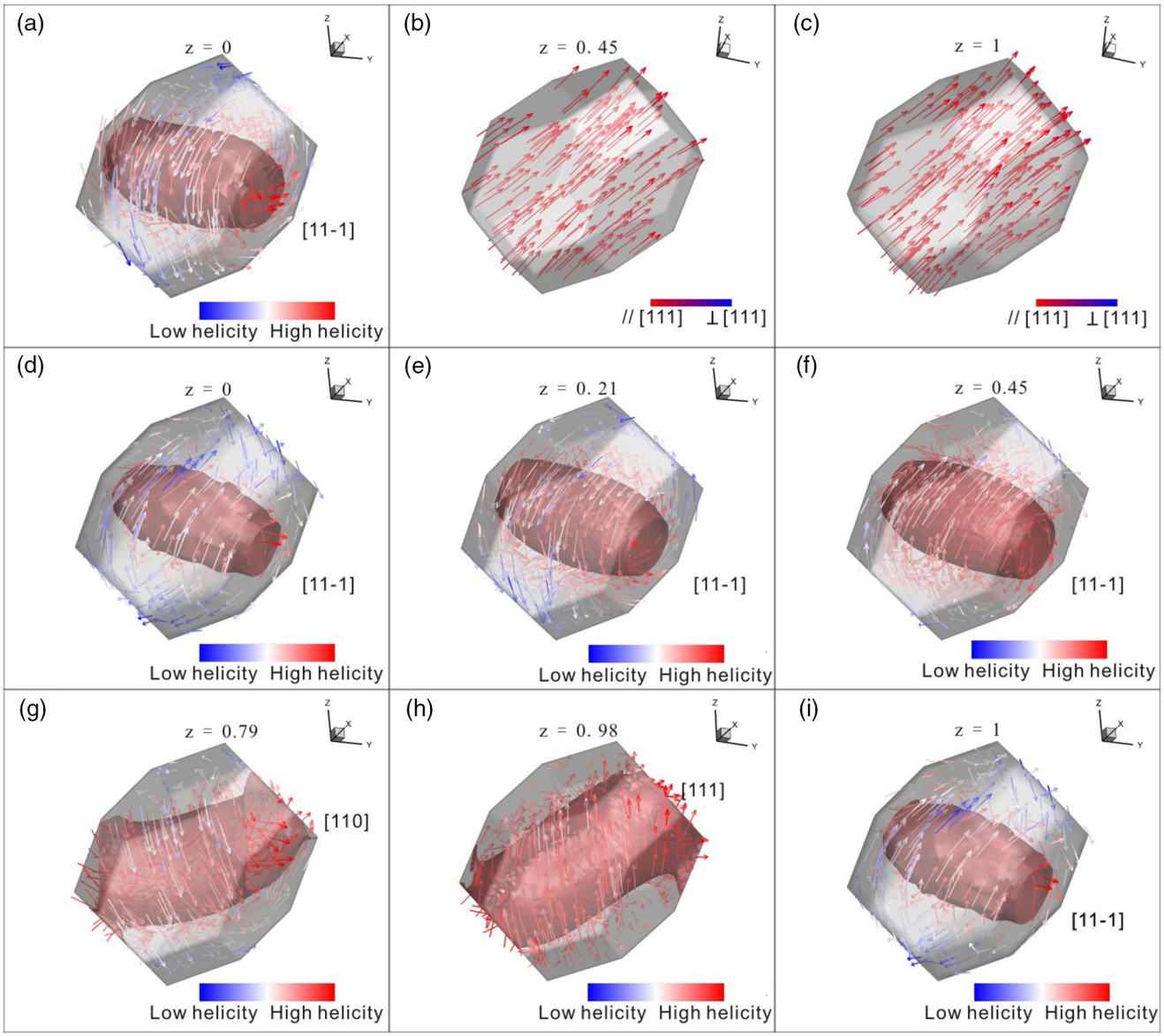

Figure 5. Micromagnetic structures of 90 nm (a)–(c) and 100 nm (d)–(i) sized grains versus oxidation parameter (z) at zero field, namely $z = 0$, 0.45, and 1 for 90 nm, and $z = 0$, 0.21, 0.45, 0.79, 0.98 and 1 for 100 nm grain. The initial applied field for all models was a saturating field of 180 mT applied along the (111) direction. (a, d-f) display the helicity isosurfaces that correspond to the regions surrounding the vortex cores. (b)–(c) Share the same coding, with magnetization of elements aligning parallel to (111) being red and perpendicular being blue.

dispersion in high-purity kaolin, powdered samples, such as those of Dunlop (1986) have a moderate interaction spacing based on their observed M_{rs}/M_s.

Muxworthy et al. (2003) suggested that both B_c and M_{rs}/M_s decrease as a result of interparticle magnetostatic interactions in magnetic assemblies. Afremov et al. (2018) also found that magnetostatic interactions in powdered Fe/Fe_3O_4 core-shell particles decrease the coercivity and magnetization remanence. Thus, we expect the predicted averaged hysteresis parameters from numerical models to be substantially higher than those of experimental observations on powders.

In this study, the observed average grain elongation of 1.31 means that the shape anisotropy begins to dominate (Ge & Liu, 2014; Muxworthy et al., 2003; Tauxe et al., 2002). For such particles, Muxworthy et al. (2003) predicted that for near uniaxial magnetite grains of between 30 and 150 nm in size (side length of equivalent cubic volume), magnetostatic interactions in powders are likely to decrease B_c and M_{rs}/M_s

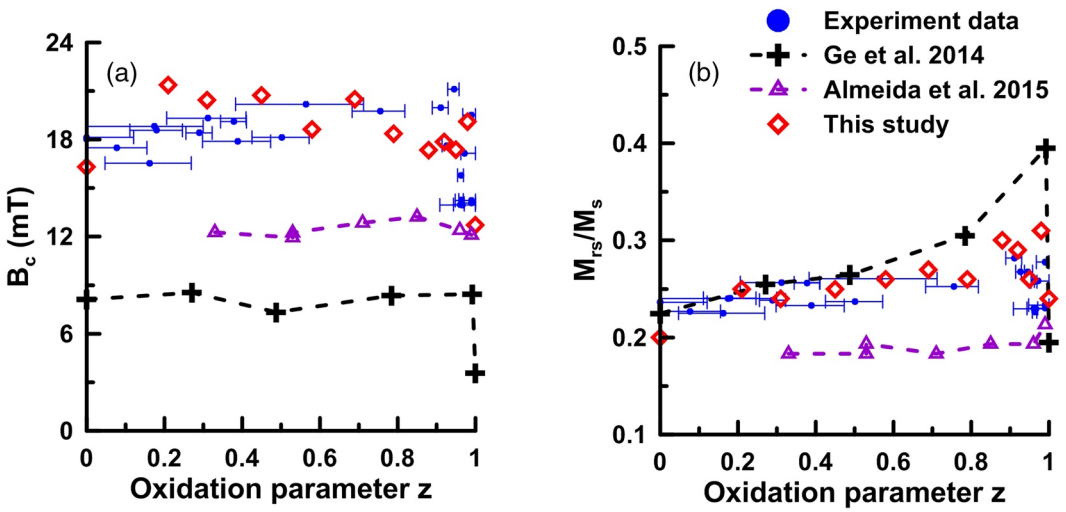

Figure 6. Weighted micromagnetic modeling results of (a) B_c and (b) M_{rs}/M_s versus oxidation parameter (z), according to the grain size distribution, in comparison with previous modeling results of Ge et al. (2014) and experiments results from Ge et al. (2014) and Almeida et al. (2015). Note that the interaction effects have been considered both in the weighted multilayer and 2-layer models.

by percentages P_h and P_m of ~17% and ~18%, respectively (Afremov et al., 2018; Fidler & Schrefl, 1996; Muxworthy et al., 2003). We might expect the dipole-dipole interaction to be proportional to the particles' decreasing saturation magnetization as the oxidation process occurs (Afremov et al., 2018; Anisimov & Afremov, 2018). Therefore, in order to simulate hysteresis behavior for a powdered sample we might reasonably apply a simple interaction field correction

$$B_{cor} = B_{ini} - B_{mag} * P_h * \left(M_{ox} / M_{mag}\right) \quad (1)$$

and similarly

$$M_{rs,cor} = M_{rs,ini} - M_{rs,mag} * P_m * \left(M_{ox} / M_{mag}\right) \quad (2)$$

where B_{ini} and $M_{rs,ini}$ are the initial coercivity and saturation remanence of oxidized magnetite calculated by the average over a lognormal distribution of grain sizes, where B_{cor} and $M_{rs,cor}$ are the counterparts after the interaction field correction, and B_{mag} and $M_{rs,mag}$ are the corresponding equivalents of stoichiometric magnetite. M_{ox} and M_{mag} are the saturation magnetization of partially oxidized and stoichiometric magnetite, respectively.

To compare the experimental data from magnetic powders with those from micromagnetic models, we create curves for the B_c and M_{rs}/M_s ratios from Figure 3 by weighting the results from different grain sizes by their proportions in the experimental data in Figure 6. The hysteresis parameters of experimental data as a function of oxidation exhibit similar behavior to that predicted from the micromagnetic models presented in this study, showing little variability in B_c and a slight increase in M_{rs}/M_s up to z = ~0.9. For larger z values, there is a dramatic drop just as the magnetite is totally oxidized. This abrupt decrease of hysteresis parameters appears both for the multilayer core-shell model of the present study as well as the previously reported 2-layer core-shell model (Ge et al., 2014), although the simpler model has much lower values for B_c. The drops are also observed in the experimental observations. Our new micromagnetic data for multilayer core-shell model has absolute values of B_c and M_{rs}/M_s that are much closer to those measured experimentally (Ge et al., 2014). In particular, the M_{rs}/M_s as a function of oxidation parameter is almost indistinguishable from the experiment results. Another group of systematic experimental data is from Almeida et al. (2015), with grains size ranging from ~150–250 nm. The variation of hysteresis parameters versus oxidation is not as evident as those for finer grains (Ge et al., 2014), resembling the modeling results for larger grains with an ESV state (Figure 3).

Note that the micromagnetic model shows a slight increase of B_c at an early oxidation stage (z values between 0 and 0.2, Figure 6a). Various experimental explanations of this increase of remanence stability have been put forward. For instance, Johnson and Hall (1978) suggested that a reduction of the effective grain size due to cracking during oxidation as a consequence of the volume change will probably increase the coercive field due to stress anisotropy. Similarly, Özdemir and O'Reilly (1982) reported that, in the absence of any other quantitatively plausible mechanism, the increase of coercivity is believed to result from such stress. They also attributed the rapid decrease near full oxidation to a decrease in the magnetostriction constant as a function of oxidation.

However, the good agreement between our micromagnetic models and experimental observations point to a radically different explanation. Both an increase in B_c with initial oxidation and a dramatic decrease before full oxidization are predicted by calling on the magnetostrictive effects of stress. The suggestion from our models is that the increase of B_c is purely due to the change in the domain structure during oxidation, in which we observe the domain states rotating from the unstable hard aligned vortex to the uniform or more stable intermediate and easy aligned vortex states during oxidation (Figure 5). Thus, the changes in coercivity and remanence are related to the dramatic changes in domain microstructures that occur by oxidizing magnetite to maghemite.

4.1. Observational Evidence of the Magnetic Unstable Zone

This study demonstrates good agreement between the experimental observations both in terms of the observed trends and absolute values of B_c and M_{rs}/M_s with oxidation state. This is a significant improvement on the previously published simple 2-layer core-shell model (Ge et al., 2014) which predicts coercivities far below the experimental data when the interaction field correction is applied (Figure 6a). Overall, microstructures of multilayer core-shell models for low temperature oxidized magnetite with a continuous transition zone show two types of magnetic behavior as follows:

(i) The SD (<~80 nm) and large SV grains (>~120 nm) share similar magnetic properties as a function of oxidation parameter (Figure 7). B_c is seen to decrease with increasing of oxidation (Figure 3), while M_{rs}/M_s remains stable or marginally increases. In both of these cases the microstructures remain constant throughout the oxidation process, either in an SD state for the smaller grains or in the easy axis aligned SV domain state close to the initial applied field direction despite of varying oxidation stage. The decrease in B_c and M_{rs}/M_s reflects the fact that the domain state remains constant during oxidation while the average composition changes to the slightly softer magnetic state during oxidization

(ii) The properties of fine SV grains (~80–~120 nm) show a dramatic evolution with oxidation, particularly prominent at the early and late stages of oxidation (Figure 6). This behavior is due to the rapid change in stability of remanence for domain states near the SD/SV grain size boundary. This is consistent with recent micromagnetic studies that have mapped out the domain state characteristics as a function of grain size and are remarkably similar across a number of different minerals (Nagy et al, 2017, 2019; Valdez-Grijalva et al., 2018). The models predict a grain size transition zone between easy aligned SD and easy aligned SV states, in which the domain states are SV but characterized by low stability and are generally not aligned along the easy axes. In equidimensional magnetite this transition zone is predicted to be between ~84 nm and 100 nm (Nagy et al., 2017), and is close to the size region of the elongated grains modeled here (equivalent to a spherical volume diameter of 99 nm–149 nm). The rapid variation in B_c and M_{rs}/M_s reflects proximity to the unstable zone and as the effective composition of the grain changes during oxidation

Ge et al. (2014) and Almeida et al. (2015) attributed the long rise and dramatic drop in hysteresis parameters with oxidation to the existence and disappearance of coupling effects between the magnetite core and maghemite shell. In this study, the strong interface anisotropy of the numerical model has been minimized by an approximately continuous oxidation transition zone, yet the predicted trend in hysteresis parameters remains unchanged. The observed hysteresis parameters represent an average of the two different types of domain state behavior integrated across the grain size distribution, with the contribution from these two classes of behavior, changing as the degree of oxidation is increased (Figure 7). Without a change in domain state with oxidation, one would expect unchanged hysteresis parameters except for a gradual magnetic softening reflecting the lower crystalline anisotropy of maghemite. However, with the increase of oxidation, the weighted hysteresis parameters of multilayer models, which closely match experimental observations, display a rise up to z = ~0.9 and a dramatic fall before total oxidation (Figure 6), especially for the M_{rs}/M_s.

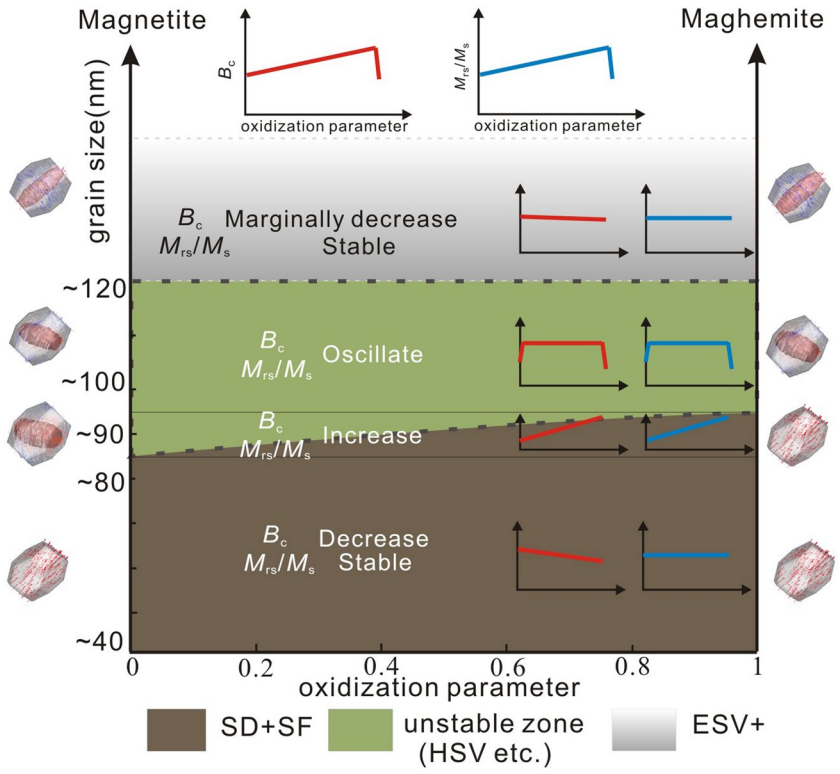

Figure 7. Sketch map of magnetic domain states for varied individual grains and oxidation parameters. The different colored areas in the figure from dark to light gray represent states of SD (single domain) + SF (single flower), unstable zone, and ESV+ (easy axis aligned SV and states for larger grains). The sketch map also shows the variation of hysteresis parameters of particles in different particle size ranges (with d of <~85, ~85–~95, ~95–~120, >~120 nm) with oxidation degree. The red and blue curves in each size range illustrate the averaged hysteresis parameters (B_c red and M_{rs}/M_s blue) versus oxidation parameter in this zone, resulting in an averaged first increase and a dramatic drop of B_c and M_{rs}/M_s of all grains as the oxidation proceeds.

The dominant contribution to the increase in hysteresis parameters can be attributed to the SD → HSV → ESV domain state changes that are predicted to occur as a function of grain size and oxidation state near 80 nm mean grain size of experimental powder samples. This is illustrated in Figure 5d and 5i which show similar $\left(11\bar{1}\right)$ vortex states aligned along the short (hard) axis of the grain for the two end members of magnetite ($z = 0$) and maghemite ($z = 1$). These represent the HSV states expected in the center of the unstable zone. For intermediate oxidized states shown in Figures 5e–5h, the vortex structure rotates toward the long (easy) axes of the grain, which the work of Nagy et al. (2017) have demonstrated are usually associated with high magnetic stability and remanence. Thus, our results are consistent with the hypothesis of a low stability zone, and that during oxidation, the domain states for the central fraction of grains in our powder sample move toward more stable structures with higher coercivity, before reverting to the unstable HSV state upon complete oxidation.

4.2. Paleomagnetic Significance and Further Studies

Paleomagnetic recordings, and in particular determination of paleointensities depend on many factors, such as choice of sample material, experimental protocols and data selection practices. These are fraught with difficulties that often reduce the success rate of observations to 20% or less (Tauxe & Yamazaki, 2015). The ability to extract the accurate field strengths relies on a number of assumptions but principally that the magnetic recording intensity is linearly proportional to the external field strength and that any given magnetic particle is magnetized and demagnetized at one specific temperature. Failure of this latter requirement can lead to magnetic recordings that are have so-called pTRM tails, whereby magnetizations acquired at one temperature require higher temperatures to demagnetize.

Whilst SD grains are thought not to be affected by pTRM tails, this has not yet been conclusively demonstrated for all SV states. Although Nagy et al. (2017), (2019) and others, have demonstrated high thermal stability and remanence for ESV, it is not true for grains near the proposed unstable zone, where multiple different domain states exist, separated by relatively low energy barriers. During thermal or ARM cycling used in stepwise paleointensity protocols, it is possible that grains near the unstable zone will change their domain state with each cycle, and so contribute to the often-observed pTRM tails that prevent accurate paleointensity determinations.

In our artificial samples, the peak of our grain size distribution is very close to the unstable zone in pure magnetite in order to maximize its effect. For equidimensional magnetite, the unstable zone is almost 50% of the stable SD range of ~40 nm–80 nm. While the SD size range will increase substantially with elongation, it is likely that the unstable zone range will also increase.

Early indications are that the unstable zone is pervasive in most magnetic materials (Nagy et al, 2017, 2019; Valdez-Grijalva et al., 2018), and further efforts are needed to fully understand their mineral magnetic characteristics. There is hope that these studies can provide a means of experimentally discriminating such domain states from the more reliable SD and ESV states and thus provides a way to improve paleointensity determinations.

5. Conclusion

Micromagnetic simulations were performed to investigate the hysteresis parameters and domain microstructures as a function of oxidation state using a multilayer core-shell model. The results show a range of variations of magnetite properties from SD to SV particles, and the averaged results based on grain size distribution are in good agreement with the experimental data both in trend and absolute values. The strong suggestion from these results is that the increase and sudden decrease in hysteresis parameters with the oxidation state is best accounted for by the rapid change in domain state that occurs near the proposed unstable zone between the SD and ESV grain size range. While there is a great deal of uncertainty in the degree to which the narrow zone of unstable vortex states might contribute to poor paleointensity determinations, the experimental observations presented here show that the rapid change in domain states with grain size near the unstable zone is consistent with experimental observations, and so form the first evidence that the unstable zone can impact magnetic properties of bulk samples. Paleomagnetic samples dominated by fine particles, such those found in chilled margins and pyroclastic rocks, though dominated by SD grains may not be immune from multiple domain state effects more commonly associated with MD states expected in larger grains.

As reliable magnetic recordings are retained by both SD and most SV grains, an effective identification method for the magnetic unstable zone should improve the way in which paleomagnetic signals can be consistently extracted from geological samples.

Data Availability Statement

The data and interpretations in this study have been uploaded into the MagIC database (Data doi: 10.7288/V4/MAGIC/17091). We thank Joshua Feinberg and two anonymous reviewers for their careful work and thoughtful suggestions that have improved this paper substantially.

Acknowledgments
This work was supported by the National Natural Science Foundation of China (Grant No. 41964003, 41964006 and 41504054) and Jiangxi Provincial Natural Science Foundation (Grant No. 20202BAB201013). We also acknowledge Natural Environment Research Council (UK) (Grant No.NE/S001018 and NE/S01197), and NSF-NERC (Grant No. EAR1827263) to W.W. and L.T.

References

Afremov, L., Anisimov, S., & Iliushin, I. (2018). Size effect on the hysteresis characteristics of a system of interacting core/shell nanoparticles. *Journal of Magnetism and Magnetic Materials*, *447*, 88–95. https://doi.org/10.1016/j.jmmm.2017.09.045

Almeida, T. P., MuxworthyKasama, A. R. T., Williams, W., Damsgaard, C., Frandsen, C., Pennycook, T. J., & Dunin-Borkowski, R. E. (2015). Effect of maghemization on the magnetic properties of nonstoichiometric pseudo-single-domain magnetite particles. *Geochemistry, Geophysics, Geosystems*, *16*, 2969–2979. https://doi.org/10.1002/2015GC005858

Almeida, T. P., Muxworthy, A. R., Kovács, A., Williams, W., Nagy, L., Conbhuí, P. Ó., et al. (2016). Direct observation of the thermal demagnetization of magnetic vortex structures in nonideal magnetite recorders. *Geophysical Research Letters*, *43*(16), 8426–8434. https://doi.org/10.1002/2016GL070074

Anisimov, S., & Afremov, L. (2018). Thermoremanent and chemical magnetization of exsolution products of nanosized titanomagnetites. *Izvestiya Physics of the Solid Earth*, *54*(1), 128–133. https://doi.org/10.1134/S1069351318010020

Bloxham, J. (2000). Sensitivity of the geomagnetic axial dipole to thermal core–mantle interactions. *Nature*, *405*(6782), 63–65. https://doi.org/10.1038/35011045

Conbhuí, P. Ó., Williams, W., Fabian, K., Ridley, P., Nagy, L., & Muxworthy, A. R. (2018). MERRILL: Micromagnetic earth related robust interpreted language laboratory. *Geochemistry, Geophysics, and Geosystems*, *19*(4), 1080–1106. https://doi.org/10.1038/35011045

Dunlop, D. J. (1986). Hysteresis properties of magnetite and their dependence on particle size: A test of pseudo-single-domain remanence models. *Journal of Geophysical Research*, *91*(B9), 9569–9584. https://doi.org/10.1029/JB091iB09p09569

Dunlop, D. J., & Özdemir, Ö. (1997). *Rock magnetism: Fundamentals and frontiers*. 8(7), (p. 573), New York, NY: Cambridge University Press. https://doi.org/10.1017/CBO9780511612794

Fidler, J., & Schrefl, T. (1996). Overview of Nd-Fe-B magnets and coercivity. *Journal of Applied Physics*, *79*(8), 5029–5034. https://doi.org/10.1063/1.361565

Gallagher, K., Feitknecht, W., & Mannweiler, U. (1968). Mechanism of oxidation of magnetite to gamma-Fe_2O_3. *Nature*, *217*, 1118–1121. https://doi.org/10.1038/2171118a0

Ge, K., & Liu, Q. (2014). Effects of the grain size distribution on magnetic properties of magnetite: constraints from micromagnetic modeling. *Chinese Science Bulletin*, *59*(34), 4763–4773. https://doi.org/10.1007/s11434-014-0584-z

Ge, K., Williams, W., Liu, Q., & Yu, Y. (2014). Effects of the core-shell structure on the magnetic properties of partially oxidized magnetite grains: Experimental and micromagnetic investigations. *Geochemistry, Geophysics, Geosystems*, *15*(5), 2021–2038. https://doi.org/10.1002/2014GC005265

Gubbins, D., Sreenivasan, B., Mound, J., & Rost, S. (2011). Melting of the Earth inner core. *Nature*, *473*(7347), 361–363. https://doi.org/10.1038/nature10068

Heider, F., & Williams, W. (1988). Note on temperature-dependence of exchange constant in magnetite. *Geophysical Research Letter*, *15*(2), 184–187. https://doi.org/10.1029/GL015i002p00184

Johnson, H. P., & Hall, J. M. (1978). A detailed rock magnetic and opaque mineralogy study of the basalts from the Nazca Plate. *Geophysical Journal International*, *52*(1), 45–64 https://doi.org/10.1111/j.1365-246X.1978.tb04221.x

Labrosse, S., Poirier, J.-P., & Mouël, J.-L. L. (2001). The age of the inner core. *Earth and Planetary Science Letters*, *190*(3), 111–123. https://doi.org/10.1016/S0012-821X(01)00387-9

Moskowitz, B. M. (1980). Theoretical grain size limits for single-domain, pseudo-single-domain and multi-domain behavior in titanomagnetite (x = 0.6) as a function of low-temperature oxidation. *Earth and Planetary Science Letters*, *47*(2), 285–293. https://doi.org/10.1016/0012-821X(80)90045-X

Muxworthy, A., Williams, W., & Virdee, D. (2003). Effect of magnetostatic interactions on the hysteresis parameters of single-domain and pseudo-single-domain grains. *Journal of Geophysical Research*, *108*(B11), 2517. https://doi.org/10.1029/2003JB002588

Nagy, L., Williams, W., Muxworthy, A. R., Fabian, K., Almeida, T. P., Conbhuiu, P., & Shcherbakov, V. P. (2017). Stability of equidimensionalpseudo-single domain magnetite over billion year timescales. *Proceedings of the National Academy of Sciences of the United States of America*, *114*, 10356–10360. https://doi.org/10.1073/pnas.1708344114

Nagy, L., Williams, W., Tauxe, L., Muxworthy, A. R., & Ferreira, I. (2019). Thermomagnetic recording fidelity of nanometer-sized iron andimplications for planetary magnetism. *Proceedings of the National Academy of Sciences of the United States of America*, *116*, 1984–1991. https://doi.org/10.1073/pnas.1810797116

O'Reilly, W. (1984). *Rock and mineral magnetism*. (p.220) Glasgow: Blackie Glasgow. Retrieved from https://link.springer.com/book/10.1007/978-1-4684-8468-7

Özdemir, Ö., & O'Reilly, W. (1982). Magnetic hysteresis properties of synthetic monodomain titanomaghemites. *Earth and Planetary Science Letters*, *57*(2), 437–447. https://doi.org/10.1016/0012-821X(82)90162-5

Özdemir, O., & Dunlop, D. J. (2010). Hallmarks of maghemitization in low-temperature remanence cycling of partially oxidized magnetite nanoparticles. *Journal of Geophysical Research*, *115*, B02101. https://doi.org/10.1029/2009JB006756

Pauthenet, R., & Bochirol, L. (1951). Aimantation spontanée des ferrites. *Journal de Physique et Le Radium*, *12*(3), 249–251. https://doi.org/10.1051/jphysrad:01951001203024900

Readman, P., & O'Reilly, W. (1972). Magnetic properties of oxidized (cation-deficient) titanomagnetites (Fe, Ti) $_3O_4$. *Journal of Geomagnetism and Geoelectricity*, *24*(1), 69–90. https://doi.org/10.5636/jgg.24.69

Santos, C. N., & Tauxe, L. (2019). Investigating the accuracy, precision, and cooling rate dependence of laboratory acquired thermal remanences during paleointensity experiments. *Geochemistry, Geophysics, Geosystems*, *19*, 1–15. https://doi.org/10.1029/2018GC007946

Schabes, M. E., & Bertram, H. N. (1988). Magnetization processes in ferromagnetic cubes. *Journal of Applied Physics*, *64*(3), 1347–1357. https://doi.org/10.1063/1.341858

Shaar, R., & Tauxe, L. (2015). Instability of thermoremanence and the problem of estimating the ancient geomagnetic field strength from non-single-domain recorders. *Proceedings of the National Academy of Sciences of the United States of America*, *112*, 11187–11192. https://doi.org/10.1073/pnas.1507986112

Shashkanov, V. A., & Metallova, V. V. (1972). Violation of Thellier's law for partial thermoremanent magnetization. *Izvestiya Physics of the Solid Earth*, *3*, 80–86. https://doi.org/10.1126/sciadv.1602306

TardunoJ, A., Cottrell, R. D., Davis, W. J., Nimmo, F., & Bono, R. K. (2015). A Hadean to Paleoarchean geodynamo recorded by single zircon crystals. *Science*, *349*(6247), 521–524. https://doi.org/10.1126/science.aaa9114

Tauxe, L., Bertram, H. N., & Seberino, C. (2002). Physical interpretation ofhysteresis loops: micromagnetic modeling of fine particle magnetite. *Geochemistry, Geophysics, Geosystems*, *3*(10), 1–22. https://doi.org/10.1029/2001GC000280

Tauxe, L., & Yamazaki, T. (2015). Paleointensities. In G. Schubert (Ed.), *Treatise on geophysics*. 2nd ed., (pp. 509–563), New York, NY: Oxford University Press. Retrieved from https://www.researchgate.net/deref/http%3A%2F%2Fdx.doi.org%2F10.1016%2FB978-044452748-6.00098-5

Valdez-Grijalva, M. A., Nagy, L., Muxworthy, A. R., Williams, W., & Fabian, K. (2018). The magnetic structure and palaeomagneticrecording fidelity of sub-micron greigite (Fe_3S_4). *Earth and Planetary Science Letters*, *483*, 76–89. https://doi.org/10.1016/j.epsl.2017.12.015

van Velzen, A. J., & Dekkers, M. J. (1999). Low-temperature oxidation of magnetite in loess-paleosol sequences: a correction of rock magnetic parameters. *Studia Geophysica et Geodaetica*, *43*(4), 357–375. https://doi.org/10.1023/A:1023278901491

Wang, H., Weiss, B. P., Bai, X.-N., Downey, B. G., Wang, J., Wang, J., et al. (2017). Lifetime of the solar nebula constrained by meteorite paleomagnetism. *Science*, *355*(6325), 623–627. https://doi.org/10.1126/science.aaf5043

Williams, W., & Dunlop, D. J. (1989). Three-dimensional micromagnetic modellingof ferromagnetic domain structure. *Nature*, *337*(6208), 634–637. https://doi.org/10.1038/337634a0

Yu, Y., Tauxe, L., & Genevey, A. (2013). Toward an optimal geomagnetic field intensity determination technique. *Geochemistry, Geophysics, Geosystems*, *5*, Q02H07. https://doi.org/10.1029/2003GC000630